Materials Today Bio 13 (2022) 100181

Contents lists available at ScienceDirect

Materials Today Bio

journal homepage: www.journals.elsevier.com/materials-today-bio

Novel glucose-responsive nanoparticles based on p-hydroxyphenethyl anisate and 3-acrylamidophenylboronic acid reduce blood glucose and ameliorate diabetic nephropathy

Qiong Ma [a], Ligong Bian [b], Xi Zhao [a], Xuexia Tian [a], Hang Yin [a], Yutian Wang [a], Anhua Shi [a,**], Junzi Wu [a,*]

[a] The Key Laboratory of Microcosmic Syndrome Differentiation, Education Department of Yunnan, Yunnan University of Chinese Medicine, Kunming, Yunnan, 650500, PR China

[b] Department of Medical Biology, College of Basic Medicine, Yunnan University of Chinese Medicine, Kunming, Yunnan, 650500, PR China

ARTICLE INFO

Keywords:
3-acrylamidophenylboronic acid
P-hydroxyphenethyl anisate
Diabetic nephropathy
Slow release
Glucose response intelligent system

ABSTRACT

An insulin delivery system that self-regulates blood sugar levels, mimicking the human pancreas, can improve hyperglycaemia. At present, a glucose-responsive insulin delivery system combining AAPBA with long-acting slow release biomaterials has been developed. However, the safety of sustained-release materials and the challenges of preventing diabetic complications remain. In this study, we developed a novel polymer slow release material using a plant extract—p-hydroxyphenylethyl anisate (HPA). After block copolymerisation with AAPBA, the prepared nanoparticles had good pH sensitivity, glucose sensitivity, insulin loading rate and stability under physiological conditions and had high biocompatibility. The analysis of streptozotocin-induced diabetic nephropathy (DN) mouse model showed that the insulin-loaded injection of nanoparticles stably regulated the blood glucose levels of DN mice within 48 h. Importantly, with the degradation of the slow release material HPA *in vivo*, the renal function improved, the inflammatory response reduced, and antioxidation levels in DN mice improved. This new type of nanoparticles provides a new idea for hypoglycaemic nano-drug delivery system and may have potential in the prevention and treatment of diabetic complications.

1. Introduction

Diabetic nephropathy (DN) is one of the most common complications of diabetes and is the main cause of chronic renal failure [1]. The incidence of DN in patients with type 2 diabetes is as high as 50% and is still rising, regardless of nationality or ethnicity [2]. At present, DN treatment drugs can be divided into two categories. The first group reduces blood glucose levels, including metformin, which is a glucagon-like peptide-1 receptor agonist [3,4]; however, there are several disadvantages, such as their short effective half-lives or large dosages required. They can reduce blood sugar levels to an extent where the hypoglycaemic effect is not enough, accelerating the occurrence and progress of DN [5,6]. Therefore, a new method to stabilise and regulate blood glucose levels over extended periods is warranted. The second group includes non-hypoglycaemic drugs, such as pentoxifylline, paricalcitol, and non-steroidal mineralocorticoid inhibitors. Although these drugs can inhibit renal inflammation, increase antioxidant levels, and prevent renal fibrosis [7–9], patients may experience gastrointestinal discomfort, cardiovascular toxicity, hypotension, and other toxic side effects [10–12]. This further highlights the need to develop drugs with few side effects, high safety, low price, and long-term use to prevent DN.

Considering that the consumption of hypoglycaemic drugs may result in fluctuations in blood glucose levels, recent studies have found that variable blood glucose levels may induce more serious renal injury in diabetes, including renal oxidative stress, leading to the apoptosis of renal mesangial cells, which can promote inflammation and damage the liver and kidney function in DN patients. In this context, scientists have developed nanoparticle-based insulin delivery systems in response to glucose stimulation [13]. Phenylboronic acid (PBA) has a more stable structure, can be easily modified, and has a low price. Therefore, compared with other glucose response intelligent systems (such as glucose oxidase, concanavalin A, and other glucose response systems),

* Corresponding author. Yunnan University of Chinese Medicine, No. 1076, Yuhua Road, Chenggong District, Kunming, Yunnan, 650500, PR China.
** Corresponding author. Yunnan University of Chinese Medicine, No. 1076, Yuhua Road, Chenggong District, Kunming, Yunnan, 650500, PR China.
E-mail addresses: 2697349858@qq.com (A. Shi), xnfz@ynutcm.edu.cn (J. Wu).

https://doi.org/10.1016/j.mtbio.2021.100181
Received 7 October 2021; Received in revised form 1 December 2021; Accepted 2 December 2021
Available online 3 December 2021

the PBA-based glucose response system has been extensively researched [14]. Studies have shown that the pKa value of PBA can be reduced by polymerizing PBA with polymer sustained-release excipients, so that PBA can react with glucose under human physiological conditions. The polymer can maintain an effective drug concentration *in vivo* for an extended time after insulin loading, which can greatly improve efficacy [15]. However, the chronic effects and long-term toxicity of drug preparations, including polymer materials generated in the post-injection degradation process, in the body are unclear [16] and has even been reported to induce oxidative stress and inflammation [17]. Therefore, it is necessary to determine the safety of related products.

Interestingly, plant-derived drugs have shown promise in the prevention and treatment of complex diseases, including DN. Botanical drugs have many advantages, such as low cost, fewer adverse reactions, and various forms. Therefore, botanical drugs are gradually becoming viable substitutes to improve DN [18,19]. Research has shown that anise, a plant food material, modulates dyslipidaemia, lowers blood glucose levels, and improves the antioxidant capacity in diabetic rats, exerting a protective effect on renal injury [20]. P-hydroxyphenylethyl anisate (HPA) is a natural compound extracted from anise. As a methoxy derivative, HPA has protective effects on the kidney as well as anti-bacterial, anti-inflammatory, and anti-oxidative activities. For example, Anna et al. [21] combined anisic acid and lysophosphatidylcholine (LPC), resulting in the formation of a covalent bond at the n-1 position. Combined 1-benzoyl-2-hydroxy-*sn*-glycerin-3-phosphate choline can improve glucose-stimulated insulin secretion (GSIS), whereas the MIN6 β pancreatic cell line can mobilise intracellular calcium to prevent and treat diabetes. In addition, Sayed et al. [22] found that anisic acid displayed protective effects on DN rats. After treatment with anisic acid for 21 weeks, blood glucose levels, renal function, and proteinuria significantly improved in DN rats. Antioxidant indices, such as superoxide dismutase (SOD), glutathione peroxidase, and catalase, increased in the renal tissue, whereas the levels of inflammatory factors, such as IL-6, decreased. These studies show that HPA performs well in the prevention and treatment of DN, which may be able to solve the adverse side effects and high prices. However, there are few reports on plant-derived drugs being directly used as biomaterials.

Based on the above, we used plant extracts to construct a new slow release material, which can be effectively combined with a glucose-responsive intelligent system for stable glucose reduction, which may treat or delay DN progression. For this reason, we esterified HPA by acryloyl chloride for long-term slow release and better safety. Following, a new polymer (AAPBA-b-HPA) was synthesised by block copolymerisation with AAPBA, which was used as a drug carrier to encapsulate insulin for nanoparticle injection. Finally, the nanoparticles were injected into DN mice to observe its preventive and therapeutic effects: detection of hypoglycaemia, protection of renal function, reduction in the inflammatory state, and oxidative stress (Scheme 1). Our new intelligent glucose-response system can provide new ideas for the prevention and treatment of patients with DN.

2. Materials and methods

2.1. Materials

2.1.1. Reagents

AAPBA was purchased from Wuhan Jusheng Technology Co., Ltd. (Beijing, PR China). Acrylic acid-HPA was purchased from Hangzhou Yuhao Chemical Industry Co., Ltd. (Hangzhou, PR China). The design plan was provided by our team, and the synthesis method used was described previously [23]. Insulin (95% purity, 27 μL/mg) was purchased from Shanghai McLean Biochemical Technology Co., Ltd. (Shanghai, PR China). Dimethyl sulphoxide (DMSO), ether, methanol, and other analytical pure solvents were purchased from the National Pharmaceutical Chemical Reagent Co., Ltd. (Shanghai, PR China). Ultra-pure water was prepared in our laboratory.

2.2. Preparation of p(AAPBA-b-HPA) polymer

2.2.1. Construction of acrylic acid-HPA

The structure of the HPA monomer was modified by acryloyl chloride esterification. The preparation scheme was as follows (Scheme 2a): tetrahydrofuran and pyridine mixed solvent with HPA was added into a four-neck flask for stirring, then acryloyl chloride (molar ratio of acrylic acid-HPA of 1:5) was added in a drop-wise manner followed by heating (50 °C, 4 h). After the reaction, acrylic acid-HPA was poured into a large amount of water and neutralised with hydrochloric acid. Then, the acrylic acid-HPA product was obtained by repeated washing and drying. Finally, the acrylic acid-HPA product with high purity was obtained via separation column, and the HPA monomer was treated to have a C═C bond. Table S1 and Table S2 show whether the modified HPA can still achieve therapeutic effects.

2.2.2. Synthesis of p(AAPBA-b-HPA) polymers

The C═C double bond of acrylic acid-HPA can be block copolymerised with the C= C double bond of p(AAPBA) to form different proportions of polymer p(AAPBA-b-HPA) via the one-pot method [24]. The synthesis of this new type of high molecular weight polymer was divided into two steps. First, the macromolecular initiator p(AAPBA) was synthesised with AAPBA as the monomer, AIBN as the initiator, and dimethylformamide (DMF) as the solvent (with a mass ratio of the initiator to AAPBA of 1:1000 and a mass ratio of solvent to AAPBA of 2:1), the resulting mixture and magnetic stirrer were sealed into a dry and clean 50 mL round bottom flask. A vacuum pump was used to pump the air out of the bottle until the mixture was stirred without air bubbles, before adding nitrogen. The latter was repeated three times before placing the flask at 70 °C in a magnetic oil bath for 12 h under the protection of nitrogen. After 12 h, the round bottom flask was removed and immediately cooled in ice water for 5 min, before adding 1 mL methanol to dissolve the polymer. Finally, the dissolved polymer was removed using a syringe, carefully placed into a beaker containing 50 mL ether, washed and precipitated, filtered and separated, and placed into a vacuum drying box for two days to obtain p(AAPBA) (Scheme 2b).

When synthesizing p(AAPBA-b-HPA), we used the same methods as described above. Using acrylic acid-HPA and p(AAPBA) as monomers, AIBN as an initiator, Na_2SO_3 to provide an alkaline environment, DMF as a solvent, and following the same steps as those used in p(AAPBA) preparation, the p(AAPBA-b-HPA) polymer was obtained (Scheme 2c). Three polymers were prepared by changing the ratio of AAPBA to HPA as: p(AAPBA-b-HPA)1: (AAPBA:HPA = 1000:200), p(AAPBA-b-HPA)2: (AAPBA:HPA = 1000:100), and p(AAPBA-b-HPA)3: (AAPBA:HPA = 1000:50).

2.3. Characterisation of p(AAPBA-b-HPA) polymers

The structure of the synthesised sample was characterised using 1H nuclear magnetic resonance (1H NMR; JNM-ECZ400S, Japan Electronics Co., Ltd). The sample synthesised by weighing 5–10 mg was completely dissolved in a deuterated reagent (1 mL) and added to a nuclear magnetic tube for hydrogen spectrum determination. The p(AAPBA) and acrylic acid-HPA solvent was treated with deuterated DMSO (1 mL), and the solvent of p(AAPBA-b-HPA) was treated with deuterium oxide (D2O) (1 mL) + sodium hydroxide deuterium (NaOH) (1 mg).

Fourier-transform infrared (FTIR) (Thermo Fisher Scientific, Hercules, USA) characterisation of acrylic acid-HPA, AAPBA, p(AAPBA), and p(AAPBA-b-HPA) was conducted. The scanning wavelength measured ranged between 400 and 4000 cm^{-1}, with a scanning interval of 2 nm/s.

A thermogravimetric analyser (TGA5500, TA Instruments Co., Ltd., Newcastle, USA) was used to observe the relationship between the quality of the measured samples and temperature. The samples (5 mg) were heated from 30 °C to 800 °C under nitrogen conditions at a heating rate of 20 °C/min. Polymer weight changes (AAPBA and acrylic acid-HPA) were analysed based on temperature. The infrared and

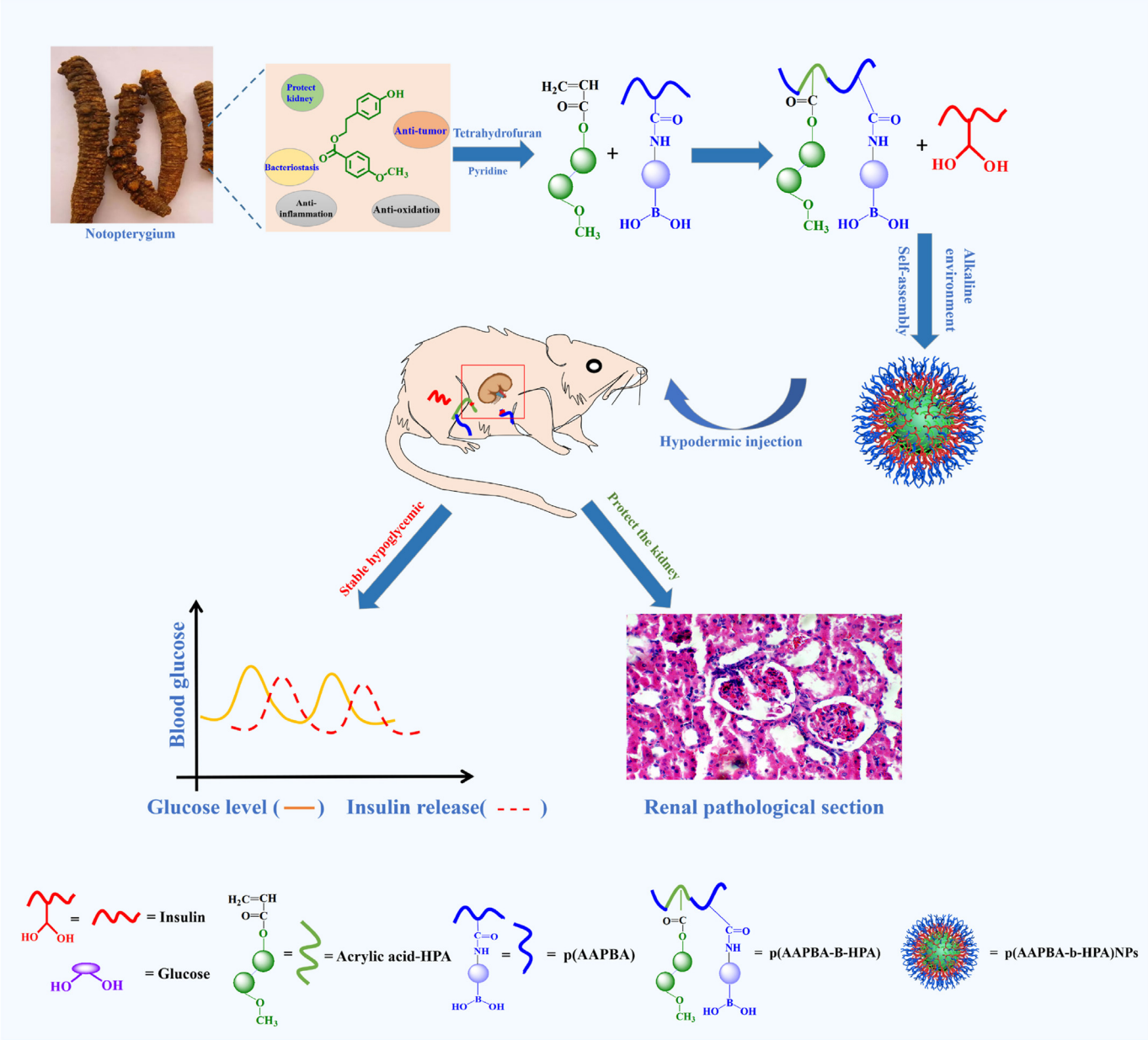

Scheme 1. Glucose-responsive delivery of insulin and release of p-hydroxyphenethyl anisate (HPA) after nano-injection.

thermogravimetric results were analysed using Origin Pro 9.0 software.

The molecular weight (Mw and Mn), molecular weight distribution, and dispersion (polydispersity index, PDI) of the polymer were determined using gel permeation chromatography (GPC) coupled with light scattering (LS) (Waters LLC, Massachusetts, USA). During the test, p(AAPBA-b-HPA) from different samples was dissolved to form a tetrahydrofuran solution of 4 mg/mL. The detection flow rate conditions were 1 mL/min with a column temperature of 35 °C.

2.4. Preparation of p(AAPBA-b-HPA) nanoparticles

The prepared p (AAPBA-b-HPA) polymer was dissolved in the mixed solvent of 100 μl methanol and placed in a shaking bed (600r/min) overnight. After it was fully dissolved, the solution was carefully added into a 50 mL beaker with 20 mL ultra-pure water (place a magnetic agitator with a rotation speed of 300 rpm/min). Tween-80 (0.5 mg) was added after 3 h, the mixture was stirred for approximately 6 h, and transferred to a dialysis bag (MWCO 6000 Da) replace with fresh DMF every 4 h, and then dialyzed with deionized water for 72 h. After dialysis, the solution was frozen overnight at −80 °C, and then freeze-dried at −65 °C for 3–4 days with a vacuum freeze dryer until the slow release excipient nanoparticle carriers of p(AAPBA-b-HPA) could be obtained.

2.5. Properties of p(AAPBA-b-HPA) nanoparticles

The morphology of the nanoparticles was observed using a JEM-2100 transmission electron microscope (TEM; Tokyo, Japan). A liquid transfer gun was used to draw 6 μL of the prepared p(AAPBA-b-HPA) nanoparticle aqueous suspension (0.4 mg/mL), which was casted on a copper grid covered with a carbon film at 38 °C for drying before observing the morphology.

Zeta potential was measured using a potential analyser (Zeta PALS/90plus, Brookhaven Instruments Corporation, New York, USA). During the determination, 0.4 mg of p(AAPBA-b-HPA) nanoparticles were weighed, 1 mL deionized water was added, and the mixture was poured into the sample tube for determination.

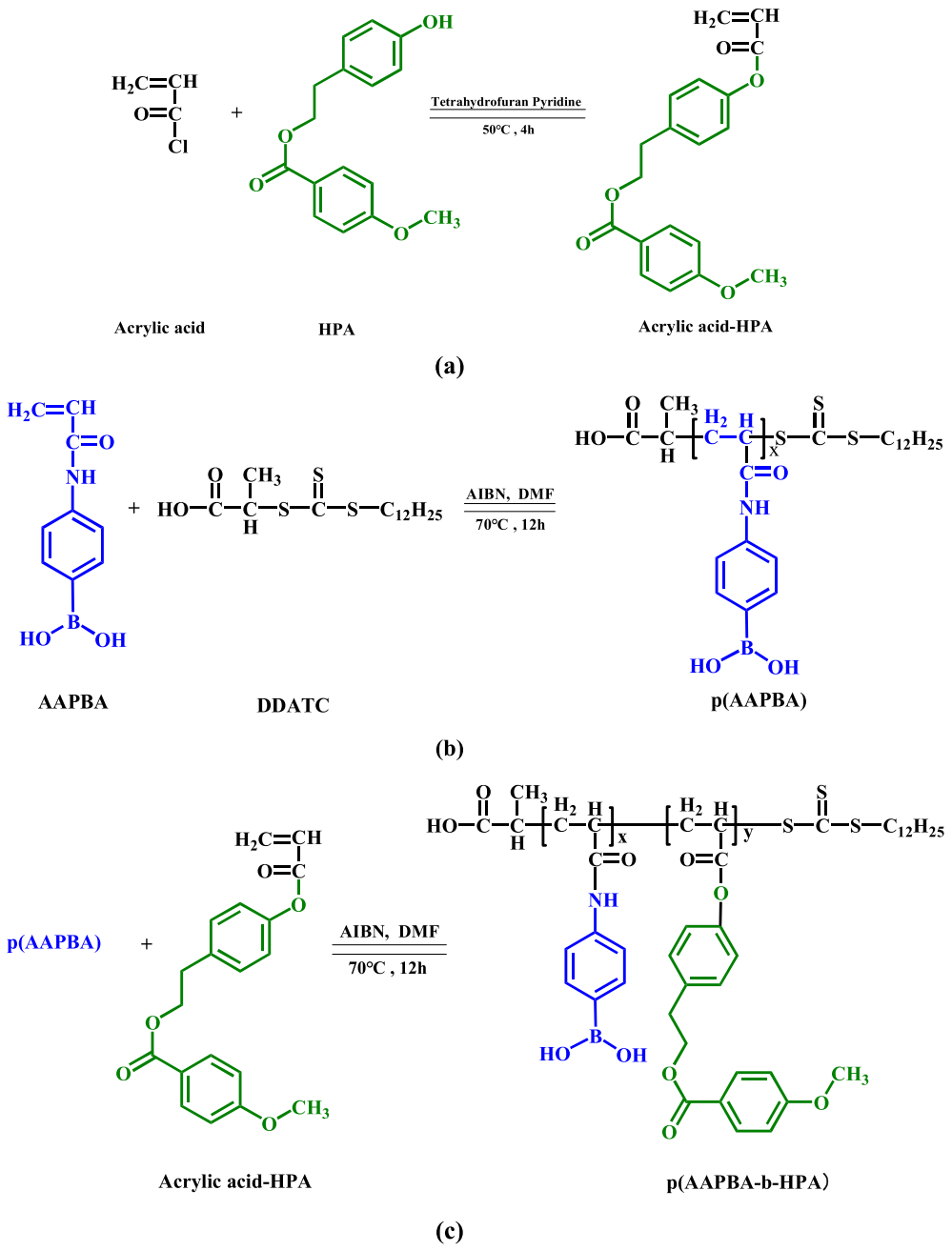

Scheme 2. Synthesis of molecular structure of acrylic acid-HPA **(a)**, p(AAPBA) **(b)**, and p(AAPBA-b-HPA) **(c)**.

Dynamic Light Scattering (DLS) was used to detect a change in the nanoparticle size in simulated body fluids (SBFs) with different glucose concentrations (the main ion concentration of SBFs is shown in Table S3). The sample tubes were oscillated continuously at a speed of 80 rpm at 37 °C. The DLS was measured at pre-set time intervals, and the dialysis was continued to record the changes in the particle size with various pH sensitivity (i.e. 6.0, 6.5, 7.0, 7.5, 8.0, 8.5, 9.0, and, 9.5) by dissolving 4 mg nanoparticles in 10 mL of the PBS solution for 3 h.

p(AAPBA-b-HPA) nanoparticles (5 mg) were placed in SBFs with pH 7.4 to remove bacteria by filtration using a 0.2 μm filter for 28 d. The ambient temperature was maintained at 37 °C, and the degradation of nanoparticles was observed weekly using a projection electron microscope.

2.6. *In vitro release of insulin and HPA from p(AAPBA-b-HPA) nanoparticles*

2.6.1. *Preparation of p(AAPBA-b-HPA) nanoparticles containing insulin*

The preparation of p(AAPBA-b-HPA) nanoparticles containing insulin was as follows: 20 mg sample p(AAPBA-b-HPA) was obtained, and the subsequent steps after adding 1 mg insulin were the same as those followed for the preparation of the p(AAPBA-b-HPA) blank nanoparticles to obtain insulin-loaded nanoparticles.

$$EE = (total\ insulin\ mass - free\ insulin\ mass) \,/\, total\ insulin\ mass \times 100\%$$

$$LC = (total\ insulin\ mass - free\ insulin\ mass) \,/\, mass\ of\ nanoparticles \times 100\%$$

All measurements were repeated three times and averaged.

2.6.2. Insulin release from nanoparticles in vitro

The insulin release behaviour of insulin-coated nanoparticles in the SBF buffer with pH 7.4 was studied using dialysis. During the determination, 5 mg p(AAPBA-b-HPA) nanoparticles with different proportions were dispersed in SBFs with different sugar concentrations (0, 6, and 18 mmol/L) and pH of 7.4. The dialysate (1 mL) was extracted at pre-set time intervals, and then 1 mL of SBF with corresponding glucose concentration was replenished. After the reaction with the BCA kit (Thermo Scientific, New York, USA), the amount of free insulin was measured using a UV-Vis spectrophotometer at 562 nm. Finally, the average result was calculated.

2.6.3. HPA release from nanoparticles in vitro

The method for the determination of HPA drug release is consistent with the above-mentioned method for the determination of insulin. The HPLC determination conditions were as follows: chromatographic column: Phenomenex C18 (4.6 mm × 250 mm, 5 μm; Beijing Xianming Leshi Science and Technology Development Co., Ltd.); mobile phase: acetonitrile −1% glacial acetic acid (30:70); flow rate: 1 mL/min; detection wavelength: 257 nm; sensitivity: 0.02 AUFS. The regression equation of the UV detector set at 256 nm and 40 °C was $Y = 20464\ X + 2842$, $r = 0.9998$, with a 0.206–4.120 ng/L linear range.

2.6.4. Circular dichroism (CD) detection spectrum

The conformation of released insulin was tested using BRIGHT TIME Chirascan (Jasco-815, UK Applied Optophysics). Visible and near-ultraviolet light were used as incident light sources to obtain the molecular structural information of the photoactive groups present in insulin and to compare the secondary structure of the released insulin with that of standard insulin using CD and asymmetric molecules to analyse the difference in absorption produced by left and right circularly polarised light.

2.7. Toxicological experiments

2.7.1. Cell viability

In this study, the cytotoxicity of p(AAPBA-b-HPA) was determined using a thiazolyl bromide tetrazolium assay (MTT) to verify its biocompatibility. Human liver normal L02 cells and cancer SMMC-7721 cells were cultured in the active growth stage as experimental cells in 96-well plates at 37 °C, with 5% CO_2 for 24 h. Then, different proportions of p(AAPBA-b-HPA) aqueous solution samples (25 μL) were added to the plates, and the same amount of the PBS buffer solution (pH 7.4) was added to the first row of cells in each plate as controls. After 24 h of incubation, a 20 μL mixture of MTT and phenazine methosulphate was added to each well (20:1). After 4 h of incubation, the culture medium was carefully removed and DMSO was added, shaking the plate for 10 min to ensure that crystals were fully dissolved.

The absorbance of each well was measured (absorbance wavelength: 490 nm) using an enzyme-labelled instrument. The experiment was repeated thrice, and the cell survival rate was calculated. Cellular toxicity was evaluated according to the RGR value, based on the toxicity classification method of the American Pharmacopoeia, as shown in Table S4.

2.7.2. Animal toxicology study

Animal research procedures were conducted following the regulations from the Administration of Experimental Animals. All research protocols were approved by the Animal use and Ethics Committee of Yunnan University of Chinese Medicine (approval no.: R-062021G006) (animal certificate: KMMU 2014002).

Twenty mice weighing 19–23 g (male C57BL/6, Department of Experimental Zoology, Kunming Medical University) were adaptively fed in the animal room for one week (temperature: 20–22 °C, relative humidity: 40%–70%, and natural lighting: light and dark cycling for 12 h). Mice were randomly divided into four groups: normal control group, p(AAPBA-b-HPA)2 low-dose, medium-dose, and high-dose observation groups (n = 5). The control group received 1 mL/kg/d normal saline, and the low, middle, and high dose groups received p(AAPBA-b-HPA)2 nanoparticle solutions (10 mg/kg/d, 20 mg/kg/d, and 40 mg/kg/d, respectively). The diet, activity, hair glossiness, and death of the mice were recorded over 14 days. Mice were sacrificed after 14 days, and the blood was collected for routine blood tests (using the automatic biochemical instrument in the laboratory department of the first people's Hospital of Yunnan Province). The liver, kidney, spleen, heart, and lung were collected for HE staining, and histopathological changes were observed using a microscope (BX53 microscope, Olympus, Japan).

2.8. In vivo study of STZ-induced DN in mice

Before the experiment, the mice were fed adaptively in the animal room (temperature: 20–22 °C, relative humidity: 30%–70%, natural lighting: 12 h of light and dark cycling) for one week. Mice were randomly divided into a normal (n = 10) and model (n = 30) groups and were given high-fat and high-sugar diets (the formula was 75% normal diet + 10% lard + 12% sucrose + 2.9% cholesterol + 0.1% sodium cholate). Four weeks later, the mice in the model group were intraperitoneally injected with streptozotocin (STZ, 35 mg/kg), prepared using a sodium citrate buffer solution. The mice in the normal group were injected intraperitoneally with the corresponding volume of citrate buffer. On days 3, 5, and 7 after modelling, blood samples were collected from the abdominal aorta of two mice randomly selected from each group and urine was collected every 24 h to determine the fasting blood glucose (7 h later) and urine protein, respectively. The success criteria of the DN model were blood glucose ≥16.7 mmol/L and 24 h urinary protein ≥30 mg. The successful mice were randomly divided into three groups: DN model group (n = 10), insulin solution injection group (n = 10), and p(AAPBA-b-HPA)2 nano-injection group (n = 10). Among them, the p(AAPBA-b-HPA) of the p(AAPBA-b-HPA)2 injection group was encapsulated with 0.4 mg insulin (dissolved in 0.5 mL normal saline and then injected subcutaneously). The insulin solution for the insulin injection group consisted of 1 mg insulin dissolved in 1 mL normal saline and was administered as 0.16 mg/d. The blank and model groups were treated with the same volume of normal saline via injection.

During the experiment, the coat colour, body weight, and blood glucose of mice in each group were observed. During the continuous eight weeks of intervention, the urine of mice from each group was collected daily using a metabolic cage, and blood was collected from the tip of the tail at a fixed time point. To observe the hypoglycaemic characteristics of p(AAPBA-b-HPA)2 nano injection, changes in blood glucose and insulin levels were measured within 48 h using a blood glucose meter (GT-1640; Guilin Renke Medical Science and Technology Development Co., Ltd., Guilin, China). We further evaluated the pharmacodynamics of HPA release by p(AAPBA-b-HPA)2 nano injection during the degradation of carrier drugs. The serum and kidney tissues were collected after the mice were sacrificed. Renal tissues fixed with 4% paraformaldehyde solution were routinely embedded in paraffin, sectioned, stained with HE, and the histopathological changes were observed using a microscope. The levels of serum creatinine (SCr) and blood urea nitrogen (BUN) were detected using an automatic biochemical analyser, and the changes in the urinary protein (UTP) (24 h urinary protein quantity = urinary protein concentration × 24 h urine volume) were measured using the biuret method. The oxidation and antioxidation indices of serum malondialdehyde (MDA), total antioxidant capacity (T-AOC), glutathione (GSH), and SOD were detected using a commercial kit (Nanjing Jiancheng Institute of Biological Engineering). Serum C-reactive protein (hs-CRP), Interleukin-1 (IL-1), Interleukin-6 (IL-6), Interleukin-8 (IL-8), and tumour necrosis factor-α (TNF-α) were detected using ELISA kits.

2.9. Statistical analysis

The data were analysed using GraphPad Prism 5.0 statistical software package for one-way ANOVA. Single-factor analysis of variance was used

for comparison among more than two groups, and a *t*-test was used for comparison between two groups. A $P < 0.05$ indicated that the difference was statistically significant.

3. Results and discussion

3.1. Synthesis and characterisation of p(AAPBA-b-HPA) polymers

p(AAPBA-b-HPA) polymers were synthesised using the three-step method (Scheme 2 a, b and c), and the raw materials and polymers were analysed using 1H NMR and FTIR to determine the success of each step.

The chemical structures of raw materials and polymers were characterised using 1H NMR spectroscopy, which can further determine whether the polymerisation was successful. Fig. 1a (DMSO-d_6) δ displays following assignments for AAPBA: 5.6 (2H,1-H), 6.4 (1H,2-H), 6.1 (1H,3-H), 10.0 (1H,4-H), and 7.9–7.1 (H of benzene ring). Fig. 1b (DMSO-d_6) δ shows the following assignments for HPA: 7.10–8.12 (H of benzene ring), 5.9 (1H, 1-H), 6.11–6.15 (2H, 2-H), 6.38 (1H, 3-H), 3.63 (3H, 4-H), 3.0 (1H, 5-H), and 4.47 (1H, 6-H). Fig. 1c (NaOD + D20; pH = 9.5) δ shows the following allocation for p(AAPBA): 8.31 (1H, 4-H), 2.13 (1H, 5-H), 2.58 (H, 6-H), 2.78 (2H, 7-H), 6.65–7.81 (H of benzene ring), and 0.5.1–1.51 (H of $C_{12}H_{25}$ group). Fig. 1d (NaOD + D2O; pH = 9.5) δ indicates the following assignments for p(AAPBA-b-HPA)2: 8.31 (1H, 4-H), 3.1 (1H, 5-H), 4.52 (1H, 6-H), 3.70 (3H, 7-H), 0.51–1.51 (H of $C_{12}H_{25}$ group), and 6.45–7.78 (H of the benzene ring); the peaks at 2.49, 2.7, 2.82, and 3.57 ppm are the H peak positions on the polymer backbone. The distributions of AAPBA and p(AAPBA) spectra are consistent with that of Li et al. [25,26]. In addition, compared with AAPBA and HPA, the p(AAPBA-b-HPA)2 polymer has a characteristic monomer peak, a peak of the corresponding C═C double bond disappears, and a peak of H at a position where the main chain appears, which confirm the occurrence of a polymerisation reaction. Our results are consistent with the findings of Guo et al. [27]. In their study, a sugar polymer was successfully synthesised by p(AAPBA) and D-gluconamidoethyl methacrylate. The 1H NMR results show that the resonance signal of the proton assigned to the C═C double bond disappears completely, and a new resonance signal appears at the position of the main chain. Similarly, the successful synthesis of polymers in the study of Zheng et al. [28] shows the same characteristics, which indicate successful polymerisation in the present

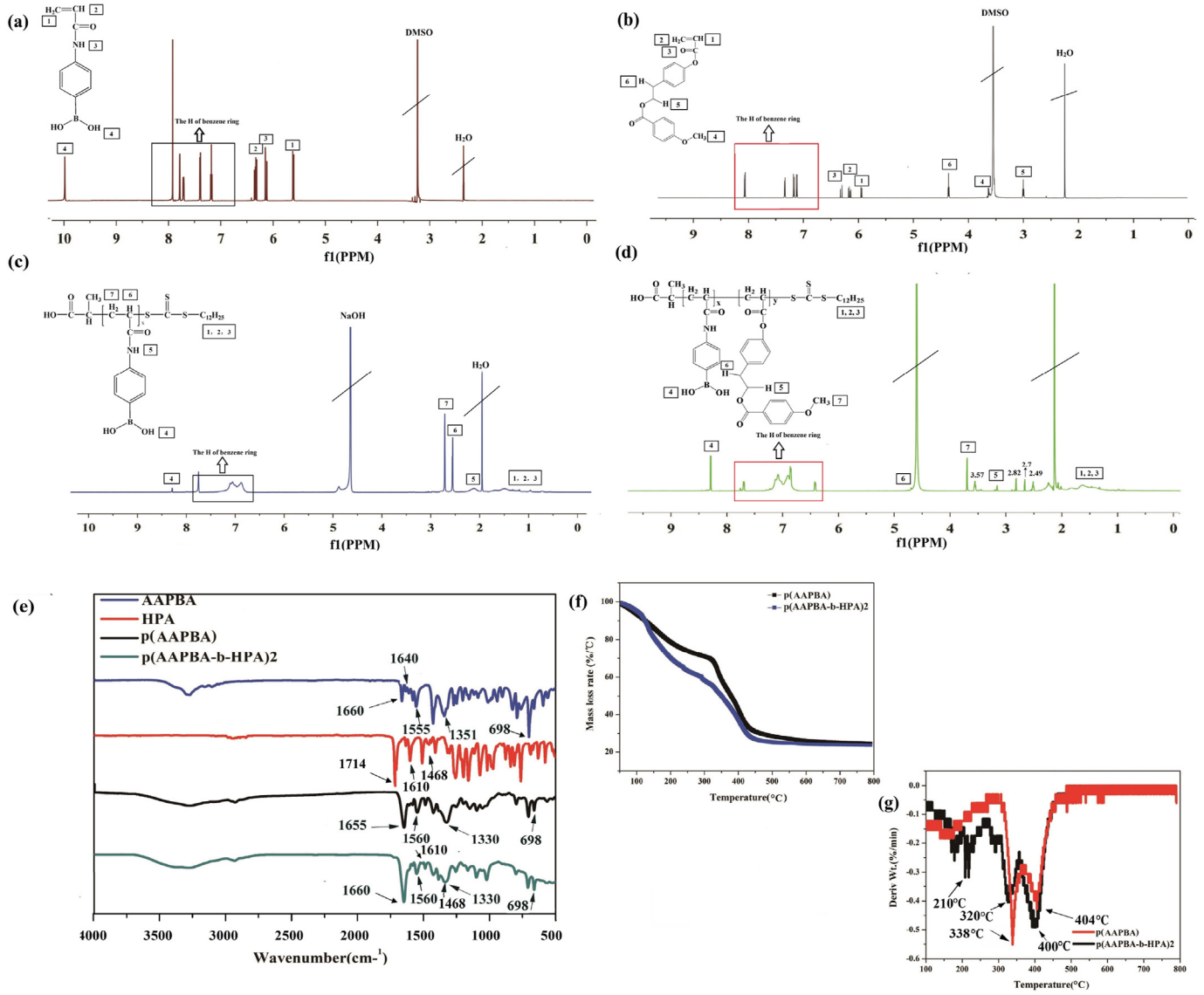

Fig. 1. 1H nuclear magnetic resonance (1H NMR) spectra of 3-acrylamidophenylboronic acid (AAPBA) **(a)**, P-hydroxyphenethyl anisate (HPA) **(b)**, p(AAPBA) **(c)**, and p(AAPBA-b-HPA). **(d)** Fourier-transform infrared (FTIR) spectra. **(e)** Thermal analysis of the polymers: thermogravimetric (TG) **(f)** and derivative thermogravimetric (DTG) **(g)**.

study.

FTIR results are shown in Fig. 1e, and the absorption bands of the AAPBA spectrum are shown as C═O tensile (1660 cm^{-1}), C═C tensile (1640 cm^{-1}), O-B-O bending (1351 cm^{-1}), and benzene ring vibration (1555–1610 cm^{-1}). There were four characteristic peaks in the HPA spectrum: CH_3 stretching (1714 cm^{-1}), C═C stretching (1630 cm^{-1}), C═O stretching (1510 cm^{-1}), and –COO stretching (1070 cm^{-1}). In the p(AAPBA) and p(AAPBA-b-HPA) spectra, the absorption caused by the C═C group disappeared, indicating successful polymerisation. The characteristic peaks of the monomers appeared in the polymer, such as CH_3 stretching (1714 cm^{-1}) and –COO stretching (1060 cm^{-1}) of HPA, C═O stretching of AAPBA (1660 cm^{-1}), and the vibration of p(AAPBA) benzene ring, indicating that HPA was successfully bound to AAPBA. Our results are consistent with those of Luo et al. [29]. In their study, after the reaction of chitosan (CS) with 3-carboxyl-4-fluorophenylboric acid (FPBA), the absorption peak of the C group of the synthesised product CS-FPBA also disappeared. In addition, Gui et al. [30] further confirmed that successfully synthesised copolymers can detect the characteristic peaks of reactant monomers.

Next, to determine whether the synthesised polymer has thermal decomposition and stability, the polymer p(AAPBA-b-HPA) was evaluated using thermogravimetric and derivative thermogravimetric (DTG) analyses. The thermogravimetric results from samples in the temperature range of 100–800 °C in a nitrogen environment (Fig. 1f) indicate that the polymer had a weight loss peak when the temperature was less than 300 °C, which might be due to the volatilisation of water. With the increase in temperature, the decomposition rate increased until combustion was completed, indicating that the p(AAPBA-b-HPA) polymer underwent thermal decomposition. DTG analysis (Fig. 1g) shows that p(AAPBA) had three mass losses at approximately 150, 338, and 404 °C, whereas p(AAPBA-b-HPA) had four mass losses at 180, 210, 320, and 400 °C. The mass loss of p(AAPBA) and p(AAPBA-b-HPA) at 150 and 180 °C, respectively, are attributed to the volatilisation of water, that at 320 and 338 °C°C, respectively, are attributed to the thermal decomposition of hanging sugar residues, that at 400 and 404 °C°C, respectively, are attributed to the thermal decomposition of the main chain, whereas the mass loss of p(AAPBA-b-HPA) at 210 °C may be due to the decomposition of hydrogen-bonded free groups.

It can be seen from the curve that the degradation temperature of p(AAPBA-b-HPA) is lower than that of p(AAPBA) due to the addition of HPA, whereas its thermal stability is improved. These observations are consistent with the thermal decomposition characteristics of AAPBA-based polymers in other studies, suggesting that p(AAPBA-b-HPA) can be used for further studies.

Finally, the molecular weight and its distribution (PDI) of the synthesised polymer were determined using GPC, as shown in Table 1. The Mw and Mn of the copolymers p(AAPBA-b-HPA)1, p(AAPBA-b-HPA)2, and p(AAPBA-b-HPA)3 increased. As proved by Li et al. [31], with the increased proportion of AAPBA, the molecular weight of the copolymer increases, and the intermolecular aggregation of nanoparticles is enhanced, roughly stabilising the PDI.

3.2. p(AAPBA-b-HPA) nanoparticle performance

The morphology and size of the nanoparticles were observed using TEM. As shown in Fig. 2, the TEM images show that before and after the treatment with 18 mmol/L glucose, the p(AAPBA-b-HPA)2 nanoparticles without insulin release (Fig. 2a) and after insulin release (Fig. 2b) are spherical, and there is no significant difference in morphology. The particle size of the nanoparticles was observed using the DLS method. From Fig. 2c, we can see that the nanoparticles are uniformly distributed and have good dispersion.

Table 1
The molecular weights (Mw and Mn) and polydispersity index (PDI) of the copolymers prepared in this work.

Samples	AAPBA/HPA mass ratio	Mw	Mn	PDI
p(AAPBA-b-HPA)1	1000:200	7.0×10^4	5.7×10^4	1.23
p(AAPBA-b-HPA)2	1000:100	7.3×10^4	5.8×10^4	1.25
p(AAPBA-b-HPA)3	1000:50	7.6×10^4	6.0×10^4	1.27

The main physical and chemical properties of nanoparticles determined are shown in Fig. 2d. It was observed that with an increase in the AAPBA ratio, the zeta potential of nano-gels became increasingly negative, which may be due to the higher hydrophobic AAPBA content, protecting them from any damage in the aqueous solution and providing relative stability. This is consistent with relevant studies [32], suggesting that p(AAPBA-b-HPA) nanoparticles are stable in aqueous solutions.

AAPBA is a Lewis acid that can react with 1mine2-or 1pyr3-diol compounds to form reversible five- or six-membered cyclic esters [33]. Therefore, when the concentration of glucose in the environment increases, the ionised PBA ions continue to combine with glucose molecules, and the balance shifts to the right, increasing the proportion of ionised AAPBA. Because the pKa value of AAPBA ranges from 8.2 to 8.6 [34], and the pH of the human physiological environment is approximately 7.4 [35], it is necessary to reduce the pKa value of the glucose-responsive PBA-based drug delivery system before the treatment of diabetes. To reduce the pKa of AAPBA and improve its response to glucose under physiological conditions, a sustained-release excipient HPA was introduced to stabilise borates through protonated groups and establish electrostatic attraction. Therefore, under physiological conditions, the PBA group in the p(AAPBA-b-HPA) polymer will combine with the dihydroxyl groups in glucose to form a hydrophilic borate structure. In addition, binding increases as glucose concentration increases, the hydrophobic polymer is converted to a hydrophilic compound, and the amphiphilic molecules are destroyed, which leads to changes in the size and glucose sensitivity of nanoparticles [36]. To confirm that the functional binding of AAPBA and HPA carriers can maintain glucose sensitivity and good stability under physiological conditions, we evaluated the characteristics of nanoparticles under different pH levels, glucose concentrations, and ultra-low temperature conditions.

Fig. 2e shows the glucose sensitivity of nanoparticles. In the SBF simulating the physiological conditions outside the human body, the particle size changes of p(AAPPA-b-HPA)1, p(AAPPA-b-HPA)2, and p(AAPPA-b-HPA)3 nanoparticles are detected at the same time interval using the DLS method with different glucose concentrations (0, 6, and 18 mmol/L). When the concentration of glucose was 6 mmol/L, the nanoparticles displayed glucose sensitivity. With the increase in glucose concentration, the size of the three samples also increased, which is due to the dissociation of more nanoparticles. At the highest glucose concentration, the particle size of nanoparticles increased significantly since the AAPBA ratio increased from p(AAPPA-b-HPA)1 to p(AAPPA-b-HPA)3. It is thus confirmed that p(AAPPA-b-HPA) nanoparticles exhibit a glucose response, and the results are consistent with the behaviour of boric acid-containing block copolymers studied by Wang et al. [37].

Fig. 2f shows the response of nanoparticles to pH. It can be observed that when the pH is 6–6.5, the nanoparticle size remains nearly unchanged. This is because the nanoparticles are electrically neutral, have no protonation, and tend to contract. Particle size began to change after pH 6.5. Further, the particle size increased as the AAPBA proportion increased in the sample. This is because a large amount of AAPBA in the polymer is ionised and the polymer is negatively charged, resulting in electrostatic repulsion between particles and increased size of the nanoparticles. These results suggest that the new nanoparticles show glucose sensitivity when the pH is 6.5, which is higher than that reported in the literature [38]. Further, the addition of HPA can reduce the pKa value of AAPBA and improve glucose sensitivity of materials under human physiological conditions.

Fig. 2g shows the stability test of nanoparticles. By storing different proportions of nanoparticles at 4 °C for 30 days, the three types are relatively stable, with insignificant size changes.

Next, we investigated the glucose elasticity of nanoparticles after

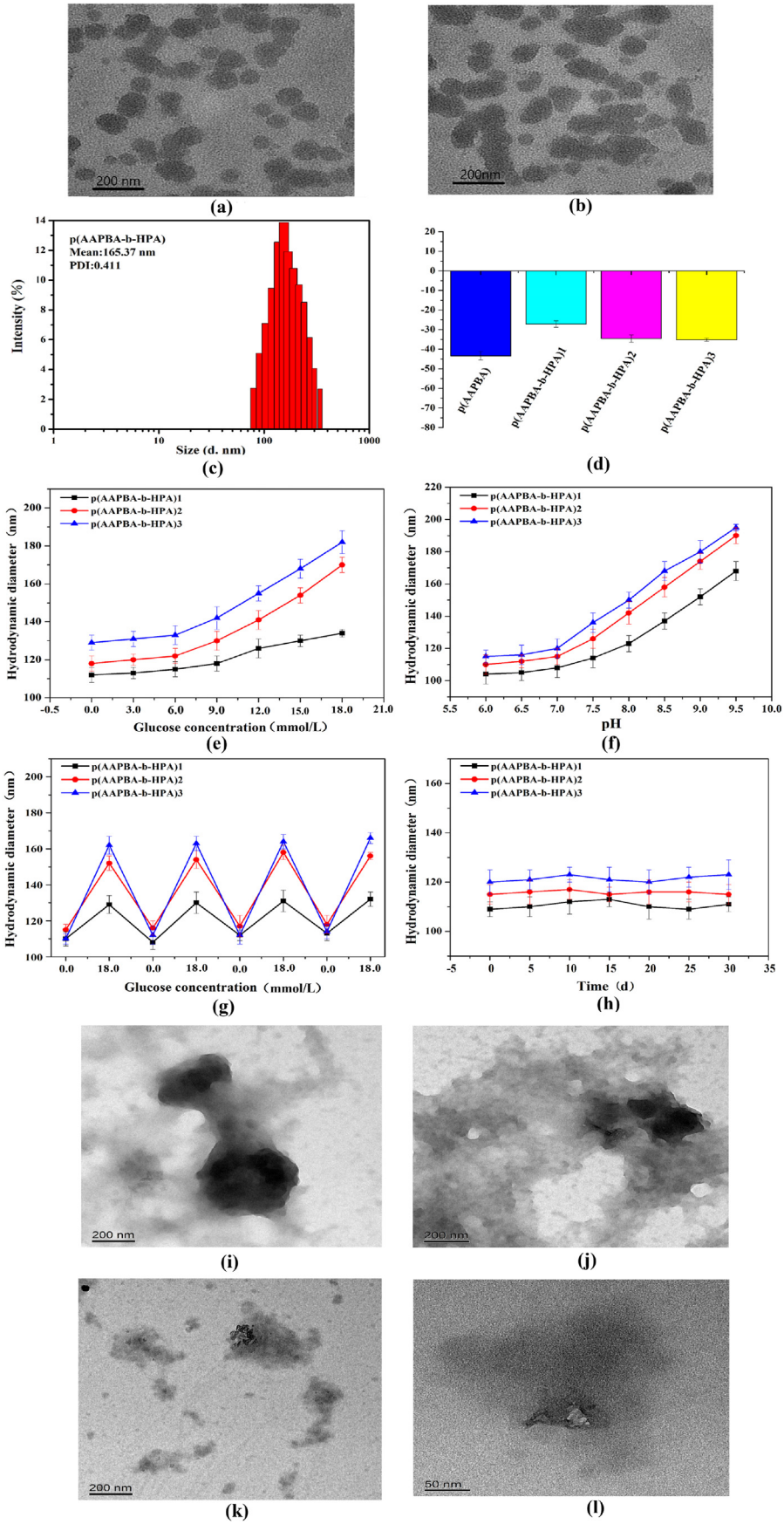

Fig. 2. Transmission electron microscopy (TEM) images of p(AAPBA-b-HPA)2 polymer nanoparticles **(a)** before and **(b)** after treatment with 18 mmol/L glucose. **(c)** The particle size and polydispersity index (PDI) of p(AAPBA-b-HPA)2 nanoparticles. **(d)** The zeta potentials of the p(AAPBA-b-HPA) nanoparticles. The different hydrodynamic diameters were as follows: **(e)** glucose concentration; **(f)** pH; **(g)** and time. **(h)** Glucose sensitive elasticity of nanoparticles. TEM showed the degradation of nanoparticles after immersion in simulated body fluids (SBF) for 7 **(i)**, 14 **(j)**, 21 **(k)**, and 28 **(l)** days.

adding and removing glucose. Since the borate ester bond between the block copolymer containing boric acid and diol is dynamically covalent, and the dynamic covalent property of borate ester promotes the reconstruction of the bond structure and boric acid bond in the presence of other competitive diols, it displays reversible glucose sensitivity [39]. Fig. 2h shows the elastic test results of three proportions of p(AAPBA-b-HPA) nanoparticles. The size of three proportions first increases and then returns to the original size after treatment with 18 mmol/L glucose for 4 h followed by dialysis with water for 24 h. As treatment time increases, the particle size increases too. This shows that nanoparticle size is glucose-dependent, which confirms their reversible glucose sensitivity, which is consistent with the performance results of the related AAPBA [40].

Biodegradability is a very important property of biomaterials. The degradation performance of materials *in vivo* often determines the success or failure of materials injected into the body [41]. Therefore, it is necessary to evaluate the degradation of biomaterials. The surface morphology of p(AAPBA-b-HPA)2 nanoparticles after soaking in SBF for 28 d is shown in the TEM images in Fig. 2i, j, 2k, and 2l. The nanoparticles displayed no obvious change in the early stage of the degradation process. After a week, the nanoparticle structure became looser, and the degradation degree of nanoparticles gradually deepened, indicating that p(AAPBA-b-HPA) nanoparticles can maintain slow and stable degradation in the simulated physiological environment. In the terms of applicability, this means that it can provide sufficient time for cell proliferation and differentiation, tissue regeneration and formation, and shows good biological activity. Therefore, when AAPBA is used as a drug carrier, it will gradually degrade and displays good safety, which is consistent with the research conducted by Zhang et al. [42].

3.3. In vitro release of insulin and HPA from p(AAPBA-b-HPA) nanoparticles

3.3.1. Release of insulin from nanoparticles

According to the above results, our nanoparticles can intelligently respond to the changes in blood glucose concentration under physiological conditions and have the potential to deliver hypoglycaemic drugs. As this treatment method has the potential to regulate the blood glucose level in diabetes, we evaluated the loading of insulin nanoparticles.

The insulin entrapment efficiency (EE) and drug loading capacity (LC) of nanoparticles are the keys to follow-up treatment evaluation, which determine the feasibility of nanoparticles as an insulin delivery system. Table 2 shows the results of drug loading and EE of insulin with different proportions of nanoparticles. It can be seen that p(AAPBA-b-HPA)1, p(AAPBA-b-HPA)2, and p(AAPBA-b-HPA)3 show good EE and LC when the amount of insulin is 1 mg. This is due to the positive and negative electric interaction of insulin during the assembly onto the nanoparticles. These interactions enable insulin to be loaded on the polymer to form a stable complex [43]. With the increasing proportions of p(AAPBA), the LC and EE of insulin significantly increased and decreased, respectively. This is related to the high number of OH groups in p(AAPBA), and the dynamic borate bond between boric acid and insulin increases the binding rate to insulin [44]. The polymers prepared herewith have shown higher drug loading rates than other AAPBA-based polymers [45], which may be due to differences in the performance of HPA materials or drug loading methods.

Next, we investigated the insulin release of nanoparticles at different glucose concentrations (0, 6, and 18 mmol/L) *in vitro*. As shown in Fig. 3a, b and c, p(AAPBA-b-HPA)1, p(AAPBA-b-HPA)2, and p(AAPBA-b-HPA)3 nanoparticles displayed rapid insulin release within the first hour. This may be because some insulin is attached to the surface of the prepared nanoparticles, hence when the nanoparticles contact the release medium, insulin is rapidly released. At the same concentration of glucose, the release order is p(AAPBA-b-HPA)3 > p(AAPBA-b-HPA)2 > p(AAPBA-b-HPA)1, which may be attributed to the increased proportion of AAPBA and mediates increased glucose binding, resulting in increased insulin dissociation. Fig. 3d shows the increasing insulin release rate of p(AAPBA-b-HPA)2 as glucose concentration increases. This is because the enhanced glucose binding under hyperglycaemic conditions leads to an increase in negative charge density in the polymer matrix, resulting in particle size changes and weakening of the electrostatic interaction between insulin and the matrix, hence the rapid release of insulin [46]. Compared to previously reported drug release rates [47], the drug release rate reported in the present study is significantly higher.

Table 2
Insulin loading capacity (LC) and entrapment efficiency (EE) of p(AAPBA-b-HPA)2 polymer nanoparticles.

Samples	Insulin concentration (mg/mL)	EE (%)	LC (%)
p(AAPBA-b-HPA)1	1.0	63.0 ± 5.1	13.4 ± 2.5
p(AAPBA-b- HPA)2	1.0	65.6 ± 5.8	16.2 ± 2.1
p(AAPBA-b- HPA)3	1.0	65.1 ± 5.4	16.3 ± 1.3

3.3.2. Release of HPA from nanoparticles

Furthermore, whether HPA can be released into the environment from the polymer with the glucose response of p(AAPBA-b-HPA) is an important condition for its pharmacological activity. As shown in Fig. 3e and f, it took approximately 20 and 10 days for p(AAPBA-b-HPA) to release HPA in 0 mmol/L or 18 mmol/L glucose solution, respectively. With the increase in glucose concentration, the HPA release rate of p(AAPBA-b-HPA)2 increases significantly. This shows that HPA release is glucose-dependent. The release characteristics of HPA from these three samples are similar to those of insulin, indicating that HPA can cooperate with insulin release to play a pharmacological role. Based on the results of the above three samples, when insulin loading is 1 mg, p(AAPBA-b-HPA)2 was selected for a follow-up study considering that it displays the best insulin release behaviour, drug loading performance, encapsulation efficiency, and cumulative release.

3.3.3. CD study of insulin released by nanoparticles

For the insulin delivery system, it is imperative to maintain the bioactive functionality of insulin, and the conformation of insulin is closely related to its biological activity [48]. We next used CD to evaluate the conformational comparison of insulin released by nanoparticles and standard insulin. The results in Fig. S1 show that the peaks at 208 and 222 mm represents the a-helix and β-structure of insulin, and both insulin have these characteristic bands (at 206 and 235 mm). These results show that the stably released insulin by nanoparticles can effectively maintain the secondary protein structure with normal biological activity.

3.4. Toxicity of nanoparticles

3.4.1. Cytotoxicity in vitro

The above studies have confirmed that our synthesised nanoparticles display great potential as a drug carrier, but it is also very important to maintain high biocompatibility when they are used to deliver insulin in patients with diabetes. We next verified whether HPA, as a new type of natural sustained-release excipients, exhibits improved biocompatibility when combined with AAPBA. The cytotoxicity of three proportions of p(AAPPA-b-HPA) nanoparticles on human normal liver L02 cells and human liver cancer SMMC-7721 cells was observed using the MTT assay to investigate the safety of the nanoparticles. The cells in the control group were untreated, whereas the cells in the treatment group were exposed to different ratios and concentrations of nanoparticles suspension, including p(AAPPA-b-HPA) low (25 μg/mL), medium (100 μg/mL), and high (125 μg/mL) treatment groups. Fig. 4a shows results from the treatment of human normal liver L02 cells. The concentration of nanosuspension increases gradually from 25 to 125 (μg/mL), but the relative proliferation rate of cells in the three groups is more than 75% with a grade I cytotoxicity, indicating that the nanoparticles are non-toxic to normal cells and cell vitality increases with increased HPA proportion.

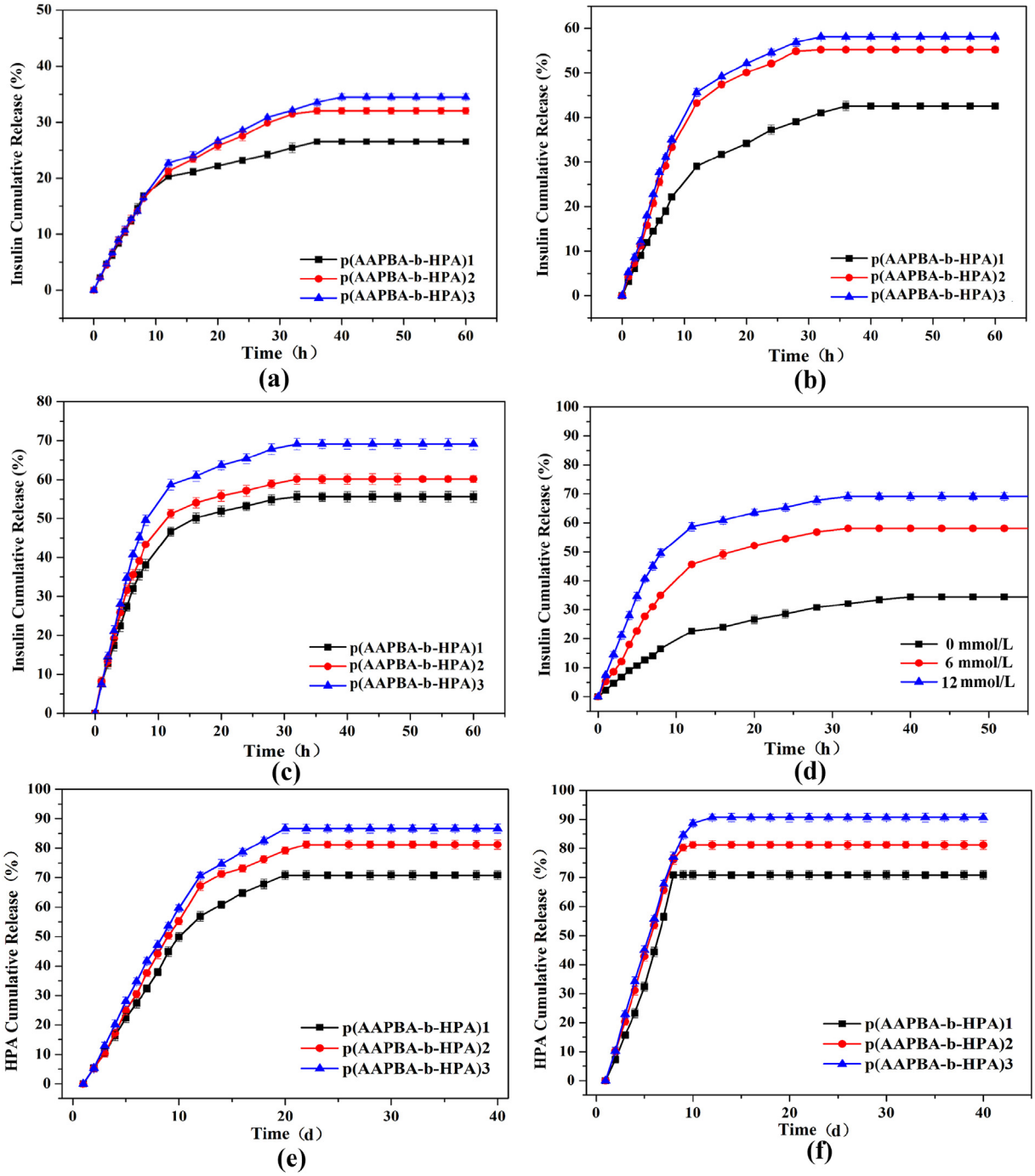

Fig. 3. Cumulative insulin release of p(AAPBA-b-HPA) nanoparticles *in vitro* with glucose concentrations of 0 mmol/L **(a)**, 6 mmol/L **(b)**, and 18 mmol/mL **(c)**. **(d)** Cumulative insulin release of p(AAPBA-b-HPA)2. Cumulative HPA release of p(AAPBA-b-HPA) nanoparticle *in vitro* with glucose concentrations of 0 mmol/L **(e)** and 18 mmol/L **(f)**.

Fig. 4b shows the results from the treatment of human hepatoma SMMC-7721 cells. With the increased concentration of nano-suspension from 25 to 125 μg/mL, the survival rate of each treatment group gradually decreased compared with that of the control group, indicating that nanoparticles exert certain toxicity to tumour cells, which may be related to the increased HPA concentrations. Studies have shown that anisic acid has cytotoxic effects on various cancer cell lines and can induce caspase-mediated apoptosis [49]. In general, these results show that the HPA in the polymer reduces the cytotoxicity of p(AAPPA-b-HPA), relatively enhancing the cytotoxicity towards tumour cells.

3.4.2. *In vivo toxicity in animals*

To further confirm the safety of HPA as slow release material, we also carried out toxicity experiments in animals to observe whether p(AAPBA-b-HPA) nanoparticles display good biocompatibility under complex drug metabolism *in vivo*. During the 14 day *in vivo* toxicity test, these mice exhibited good mental state and normal eating habits, and no mice had died during this period. After mice were sacrificed on the 14th day, the blood, liver, kidney, heart, spleen, and lung tissues were collected for testing. The toxicity results *in vivo* are shown in Fig. 4c and Supplementary Table S5. Fig. 4c shows the tissue sections of the heart, liver, spleen, lung, and kidney indicated no obvious damage to the mice during

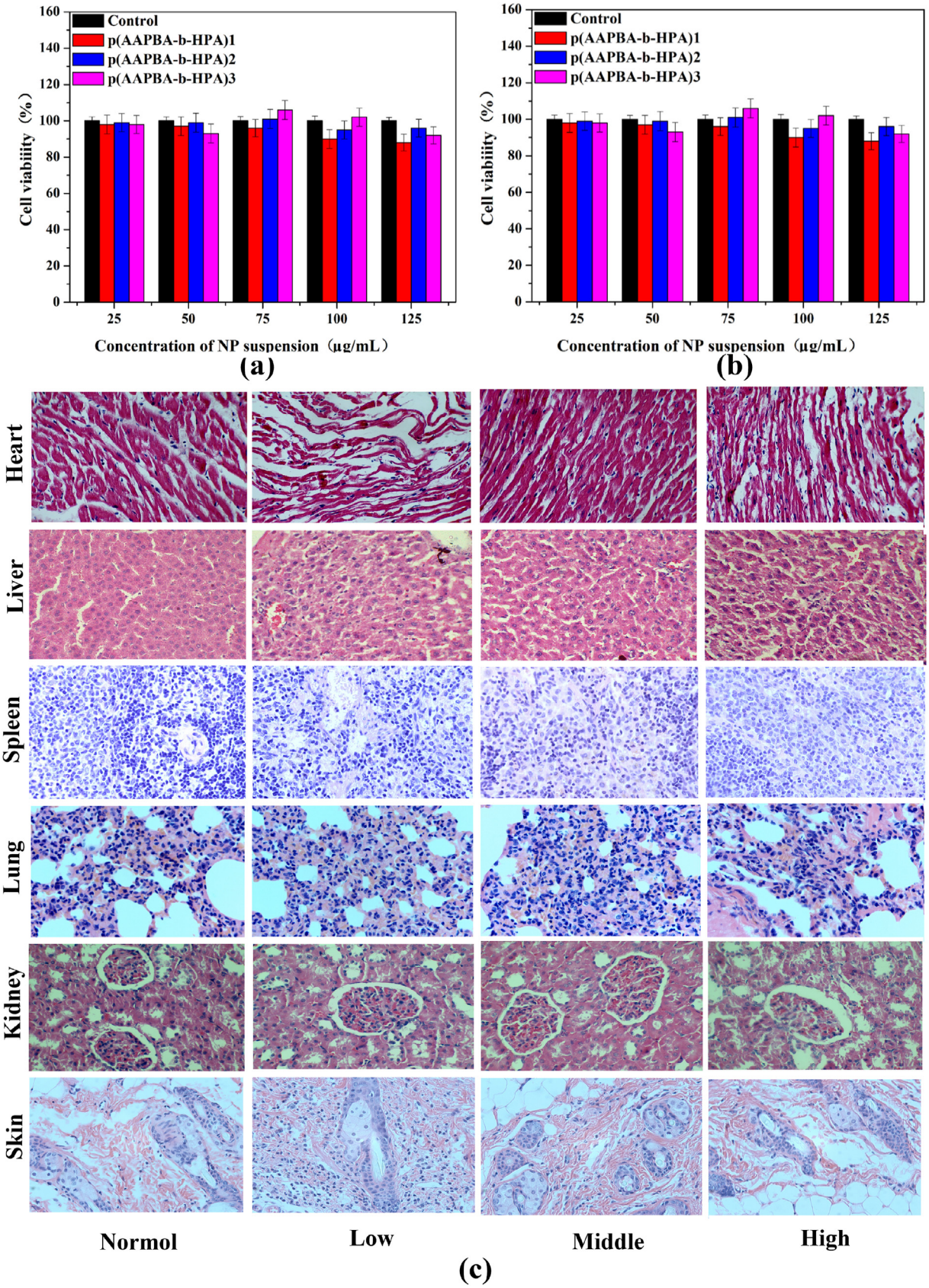

Fig. 4. **(a)**, **(b)** Cell viability as a function of the concentration of p(AAPBA-b-HPA) nanoparticle using the MTT assay at 37 °C, after incubation for 24 h. Each value represents the mean ± SD (n = 5). **(c)** HE staining representative images of heart, liver, spleen, lung, kidney, and skin in the normal group, (AAPBA-b-HPA)2 nanoparticle Low, Middle, and High treatment groups.

the 14 d injection period. Table S5 shows no significant change in blood biochemical indices between the control group and the treatment groups 14 days after injection. Taken together, the results *in vivo* and *in vitro* show that the prepared materials are safe and can be used for extended time periods, which provides a basis for the study of insulin-loaded nanoparticles and hypoglycaemic experiments *in vivo*.

In addition, we evaluated the biocompatibility of the nanoparticles in the injected skin tissue. Four days after injection, the skin tissue at the injection site showed slight redness and swelling, which is a normal phenomenon when biomaterials are injected into the subcutaneous skin. The image taken on the 14th day after the injection of nanoparticles is shown in Fig. 4c. The results of HE staining of skin tissue show that there is rarely any substantial inflammation in the tissue, which is similar to the image from the normal group. This is consistent with the literature reports of AAPBA nano injection, which does not produce an inflammatory reaction at the injection site [50]. It also further indicates that our nano injection is a safe and effective strategy with potential application value for safe *in vivo* insulin delivery.

3.5. Evaluation of hypoglycaemia characteristics and HPA pharmacodynamics of nanoparticles in DN mice

3.5.1. Hypoglycaemic properties of nanoparticles in vivo

As a slow release adjuvant, HPA can slow release the loaded drug for an extended time, prolong the effective time of the drug, and delay the half-life. Studies have shown that the occurrence of DN is closely related to hyperglycaemia, but generally oral and injection hypoglycaemic drugs have short half-lives and are prone to blood glucose fluctuations, which may accelerate the occurrence and development of DN [51]. Therefore, if the drug can stably control blood glucose levels, it can significantly delay the development of DN. The experiment evaluated whether p(AAPBA-b-HPA)2 nanoparticles can solve this problem and realise the ability of self-regulating insulin release to lower blood glucose levels in mice. The animal model of diabetes induced by a high-fat and high-sugar diet plus intraperitoneal injection of STZ was established, and different samples were injected subcutaneously: (1) normal group, subcutaneous injection of normal saline; (2) DN group, subcutaneous injection of saline; (3) insulin injection group, subcutaneous single injection of insulin; (4) p(AAPBA-b-HPA)2 groups, subcutaneous injection. The blood glucose regulation levels of the four groups were carefully monitored after injection. As shown in Fig. 5a, the blood glucose level in the model group was significantly higher than that in the normal group. Compared with the model group, each treatment group rapidly decreased the hyperglycaemic index to the upper limit of normal blood glucose within 1 h of injection. However, for some time, the blood glucose level in the insulin injection group was slightly lower than the lowest level of normal blood glucose, and normal blood glucose levels were maintained for 4 h. Compared with the insulin injection group, the p(AAPBA-b-HPA)2 treatment group maintained stable blood glucose levels for approximately 28 h. The hypoglycaemic effect observed in the p(AAPBA-b-HPA)2 treatment group was of a much longer duration than that observed in the insulin injection group, indicating that HPA sustained-release excipients can effectively prevent the rapid release of insulin and avoid excessive reduction in blood glucose levels. This shows that nanoparticles can exhibit good self-regulation and release of insulin *in vivo*, which is similar to the physiological regulation of blood glucose in healthy mice, to avoid excessive fluctuations in blood glucose.

3.5.2. HPA pharmacodynamic evaluation of the release of nanoparticles

The above experiments have proved that HPA as a sustained-release excipient has good biocompatibility and long-term sustained-release properties. Therefore, we next evaluated the pharmacological effect of HPA on DN mice. We aimed to observe whether HPA released during the degradation of p(AAPBA-b-HPA)2 can exert its pharmacological activity, protect renal tissue and renal function, reduce oxidative stress and inflammatory reaction, and improve the pathological damage of renal tissue structure in experimental DN mice. In our experiment, the DN mouse model was established using a high-fat and high-glucose diet and intraperitoneal injection of STZ. After eight weeks of subcutaneous injection, different proportions of injection of nanoparticles and insulin were injected. Thereafter, we determined the levels of related indices in serum, urine, and tissue of mice, and pathological changes in kidneys were detected to confirm the therapeutic effect of p(AAPBA-b-HPA) injection of nanoparticles in DN mice.

First, we examined whether different samples of nano-subcutaneous injection improved renal histopathological changes in DN mice. Fig. 5b shows that kidney tissues of mice were stained with HE, and the morphology was observed using a microscope. The renal tissue structure of the blank control group was normal, there was no inflammatory cell infiltration, and there were no obvious pathological changes in the glomerular sac, vascular loop, and basement membrane. The renal tubular epithelial cells of the model group appeared detached and accompanied by edema, marked mesangial cell proliferation, and significant thickening of the basement membrane in most glomeruli. Mouse kidneys displayed significant lesions and tissue structure damage after modelling, which proved that the DN model was established successfully [52]. Although the insulin treatment controlled the blood glucose of the mice, the treatment could not better prevent the occurrence of complications. As shown in Fig. 5 (b), it was observed that the basement membrane in the kidney tissue of the insulin group was thicker than that in kidney tissue of the normal group, and the pathological improvement was not significant in the insulin group. Fig. 5 (b) nano-injection group shows that the degree of pathological injury in the kidneys of mice improved significantly after intervention in the nano-injection group.

Persistent proteinuria and progressive decline of renal function are the main characteristics of DN [53], therefore, we observed renal function indicators and 24 h urinary protein quantitative markers (UTP) to determine the improvement of renal function and proteinuria. As shown in Fig. 5c and d, the levels of SCr and BUN in the model group were significantly higher than those in the normal group. Renal function indices in the insulin treatment group were improved compared with those in the model group, whereas the abnormal renal function parameters, such as SCr and BUN, in the p(AAPBA-b-HPA)2 group were significantly improved compared with those in the model group ($P < 0.05$). In addition, the p(AAPBA-b-HPA)2 treatment improved renal function to a greater degree than the insulin treatment. Some studies have shown that the determination of urinary microalbumin can better predict the occurrence of early DN, and the determination of UTP has become the main index for the diagnosis of renal injury [54]. The UTP inspection results of each group of mice are shown in Fig. 5e. From the results, it can be seen that the UTP level in the model group was significantly higher than that in the normal group, and the UTP level gradually increased with time ($P < 0.05$). Compared with those in the model group, the mice in the treatment group improved, and over time, the effect of the nanoparticle injection improved compared to the effects observed in the insulin group ($P < 0.05$). It can be seen that the combination of insulin-loaded p(AAPBA-b-HPA)2 nanoparticles has a greater potential to prevent DN and control blood glucose than insulin alone.

We further investigated the mechanism underlying the effect of p(AAPBA-b-HPA) on the prevention and treatment of DN in mice by increasing the levels of antioxidation and inhibiting inflammation *in vivo*. Literature indicates that oxidative stress can cause irreversible damage to the cellular structure and function of the kidney, the inflammatory factors are widely involved in the pathogenesis of DN [55]. Hs-CRP is an acute phase reaction protein. When insulin resistance occurs in the body, hs-CRP synthesis increases, especially after renal damage in patients with diabetes [56]. IL-1, IL-6, and IL-8 can mediate inflammatory responses through cellular and humoural immunity and play an important role in the synthesis of CRP in hepatocytes [57]. TNF-α, synthesised and secreted by mononuclear macrophages, is an important mediator of inflammatory response and a variety of pathophysiological processes. It can play an immunomodulatory role at low levels and cause pathological damage at

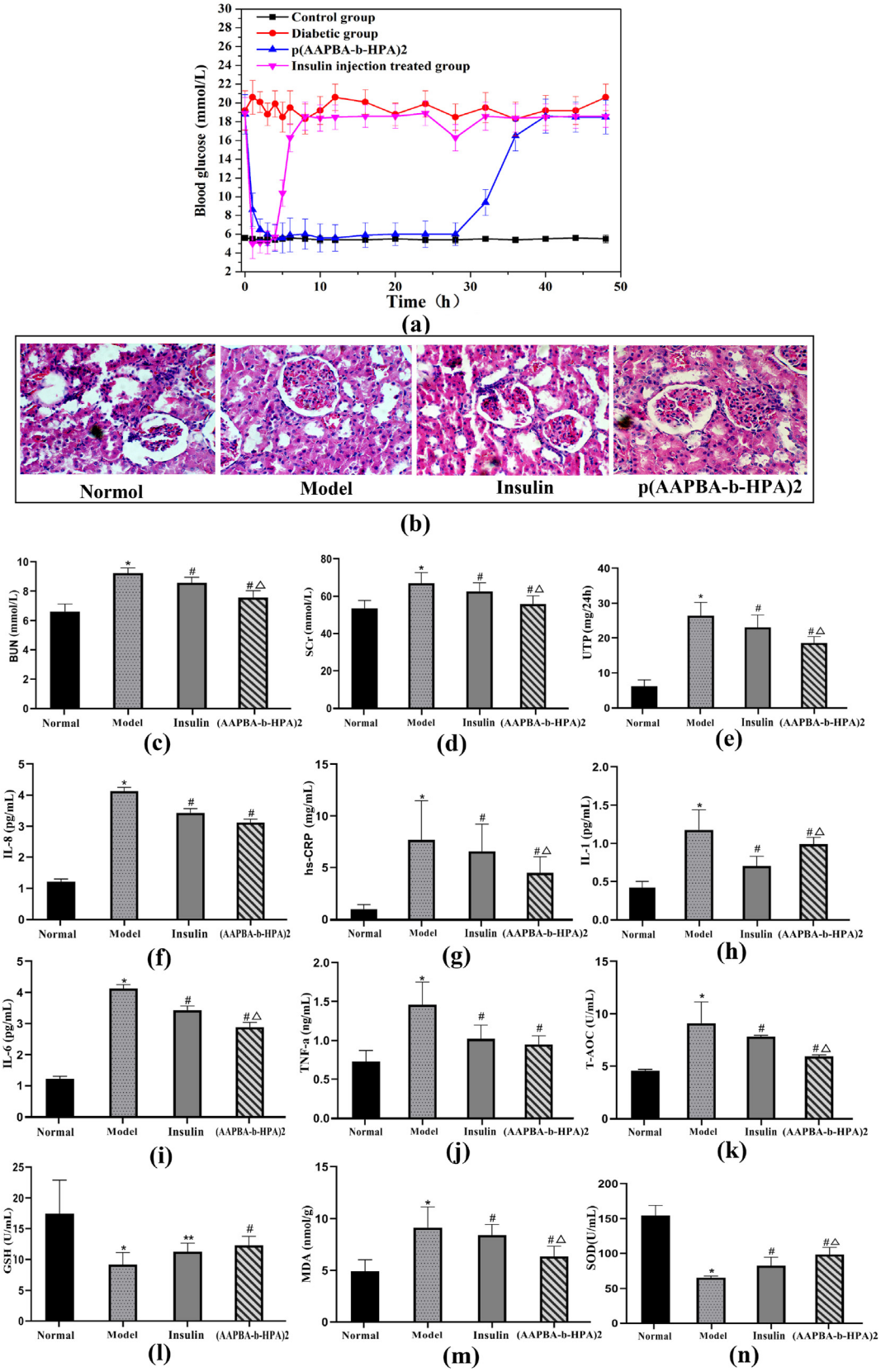

Fig. 5. **(a)** Blood glucose concentration after injection over 28 h. **(b)** Pathological changes in renal tissue of mice in each group using HE staining (× 400). The levels of BUN **(c)**, SCr **(d)**, and UTP **(e)** in each group of mice. After intervention for eight weeks, the inflammation **(f-j)** and oxidative stress indexes **(k–n)** of mice in each group were measured. Data are presented as mean ± S.D. (n = 10). $^{*}P < 0.05$ vs Normal group; $^{\#}P < 0.05$ vs Model group. $^{\triangle}P < 0.05$ vs Insulin group.

high levels [58]. Changes in inflammatory factors, such as TNF-α, IL-1, IL-6, IL-8, and hs-CRP, in the serum of mice in each group were detected using ELISA. Results shown in Fig. 5f, g, h, i, and j indicate that the levels of inflammatory cytokines in the insulin group and p(AAPBA-b-HPA) group were lower than those in the model group ($P < 0.05$), and the level of inflammatory cytokines in the p(AAPBA-b-HPA)2 group were higher than those in the insulin treatment group ($P < 0.05$). Oxidative and antioxidant indices, such as SOD, T-AOC, MDA, and GSH, can reflect the oxidative stress damage in the kidney. Fig. 5k, l, m, and n shows changes in SOD, T-AOC, GSH-PX, and MDA levels in serum of DN mice treated with p(AAPPA-b-HPA) 2 subcutaneous injection for eight weeks. Serum SOD, GSH, and T-AOC levels in the DN model group decreased significantly compared with those in the normal group, whereas MDA levels increased significantly ($P < 0.05$) in the DN model group compared with those in the normal group. SOD, GSH, and T-AOC levels in the insulin and p(AAPBA-b-HPA) groups were significantly higher ($P < 0.05$) than those in the DN model group, whereas MDA levels were significantly lower than those in the DN model group. Among them, the antioxidant effects observed in the p(AAPBA-b-HPA)2 treatment group were stronger than those observed in the insulin group ($P < 0.05$).

These results show that compared with insulin therapy alone, p(AAPBA-b-HPA)2 treatment group combined with insulin and HPA had better preventive and therapeutic effects on DN.

4. Conclusion

Taken together, our results show that this new glucose-responsive intelligent system with HPA as a sustained-release adjuvant is very reliable for the prevention and treatment of DN. p(AAPBA-b-HPA) prepared by block copolymerisation of acrylic acid-HPA and AAPBA displays good pH sensitivity, glucose sensitivity and stability under physiological conditions, and its glucose-sensitive behaviour is reversible. Polymer nanoparticles are safe, can be used for extended time periods, display low toxicity to normal cells, and exert certain inhibitory effects on tumour cells. Simultaneously, polymer nanoparticles do not exert toxic damage to the heart, liver, spleen, lung, kidney, and serum biochemical indices of mice, and are safe for skin tissue at the injection site. In addition, nanoparticles can slowly release insulin and HPA. p(AAPBA-b-HPA) nanoparticles can release HPA and insulin according to changing glucose concentrations, with high encapsulation efficiency and loading capacity of insulin, and released insulin maintains normal conformation and biological activity. Finally, nanoparticle injections can steadily reduce the blood glucose levels of DN mice up to 28 h, and with the degradation of sustained-release excipients *in vivo*, the released HPA can play its pharmacological role, improve the renal function and renal histopathology of DN mice, reduce inflammatory reactions and oxidative stress, and protect the kidney of DN mice. In conclusion, this study suggests that the copolymer of HPA sustained-release excipients and AAPBA can be used as a new self-regulating glucose response intelligent system in the future, is of great significance to reduce the incidence of DN in patients with type 2 diabetes and may have potential in the field of polymer sustained-release excipients.

Author contributions

Qiong Ma: Methodology, Writing – original draft. Ligong Bian: Data curation, Software, Formal analysis, Xi Zhao: Visualization, Investigation., Xuexia Tian: Supervision, Software, Data curation. Hang Yin:Supervision, Data curation. Yutian Wang:Software. Anhua Shi: Writing – review & editing. Junzi Wu: Conceptualization, Writing – review & editing.

Data statement

All data generated or analysed during this study are included in this published article.

Declaration of competing interest

The authors declare that they have no conflict of interest.

Acknowledgements

This investigation was supported by the Yunnan Province Natural Science Foundation Project (202101AT070274) and Young Scientists Fund of the National Natural Science Foundation of China (82104403).

Appendix A. Supplementary data

Supplementary data to this article can be found online at https://doi.org/10.1016/j.mtbio.2021.100181.

References

[1] N. Papadopoulou-Marketou, S.A. Paschou, N. Marketou, et al., Diabetic nephropathy in type 1 diabetes, Minerva Med. 109 (2018) 218–228, https://doi.org/10.23736/S0026-4806.17.05496-9.
[2] S. Oltean, R. Coward, M. Collino, et al., Diabetic nephropathy: novel molecular mechanisms and therapeutic avenues, BioMed Res. Int. 2017 (2017), 3146524, https://doi.org/10.1155/2017/3146524.
[3] E. Sanchez-Rangel, S.E. Inzucchi, Metformin: clinical use in type 2 diabetes, Diabetologia 60 (2017) 1586–1593, https://doi.org/10.1007/s00125-017-4336-x.
[4] R. Gentilella, V. Pechtner, A. Corcos, Glucagon-like peptide-1 receptor agonists in type 2 diabetes treatment: are they all the same, Diabetes Metabol. Res. Rev. 35 (2019), e3070, https://doi.org/10.1002/dmrr.3070.
[5] J. Thrasher, Pharmacologic management of type 2 diabetes mellitus: available therapies, Am. J. Med. 130 (2017) S4–S17, https://doi.org/10.1016/j.amjmed.2017.04.004.
[6] L.J. McCreight, C.J. Bailey, E.R. Pearson, Metformin and the gastrointestinal tract, Diabetologia 59 (2016) 426–435, https://doi.org/10.1007/s00125-015-3844-9.
[7] M. Al-Nimer, R. Ratha, T. Mahwi, Pentoxifylline improves the quality of life in type-2 diabetes foot syndrome, Pak. J. Med. Sci. 35 (2019) 1370–1375, https://doi.org/10.12669/pjms.35.5.11.
[8] O.M. Ahmed, T.M. Ali, M.A. Abdel, et al., Effects of enalapril and paricalcitol treatment on diabetic nephropathy and renal expressions of TNF-α, p53, caspase-3 and Bcl-2 in STZ-induced diabetic rats, PLoS One 14 (2019), e0214349, https://doi.org/10.1371/journal.pone.0214349.
[9] O. Dhaybi, G.L. Bakris, Non-steroidal mineralocorticoid antagonists: prospects for renoprotection in diabetic kidney disease, Diabetes Obes. Metabol. 22 (2020) 69–76, https://doi.org/10.1111/dom.13983.
[10] D.J. Webb, B. Coll, H.J.L. Heerspink, et al., Longitudinal assessment of the effect of atrasentan on thoracic bioimpedance in diabetic nephropathy: a randomized, double-blind, placebo-controlled, Trial. Drugs RD. 17 (2017) 441–448, https://doi.org/10.1007/s40268-017-0201-0.
[11] G. Avila, D.S. Osornio-Garduño, E.B. Ríos-Pérez, et al., Functional and structural impact of pirfenidone on the alterations of cardiac disease and diabetes mellitus, Cell Calcium 56 (2014) 428–435, https://doi.org/10.1016/j.ceca.2014.07.008.
[12] Y.C. Lin, Y.H. Chang, S.Y. Yang, et al., Update of pathophysiology and management of diabetic kidney disease, J. Formos. Med. Assoc. 117 (2018) 662–675, https://doi.org/10.1016/j.jfma.2018.02.007.
[13] A. Nusca, D. Tuccinardi, M. Albano, et al., Glycemic variability in the development of cardiovascular complications in diabetes, Diabetes Metabol. Res. Rev. 34 (2018), e3047, https://doi.org/10.1002/dmrr.3047.
[14] Q. Ma, X. Zhao, A. Shi, et al., Bioresponsive functional phenylboronic acid-based delivery system as an emerging platform for diabetic therapy, Int. J. Nanomed. 12 (2021) 297–314, https://doi.org/10.2147/IJN.S284357.
[15] X. Zhao, A. Shi, Q. Ma, et al., Nanoparticles prepared from pterostilbene reduce blood glucose and improve diabetes complications, J. Nanobiotechnol. 27 (2021), 191, https://doi.org/10.1186/s12951-021-00928-y.
[16] K. Knop, R. Hoogenboom, D. Fischer, et al., Poly(ethylene glycol) in drug delivery: pros and cons as well as potential alternatives, Angew Chem. Int. Ed. Engl. 49 (2010) 6288–6308, https://doi.org/10.1002/anie.200902672.
[17] R. Langer, H. Brem, D. Tapper, Biocompatibility of polymeric delivery systems for macromolecules, J. Biomed. Mater. Res. 15 (2) (1981) 267–277, https://doi.org/10.1002/jbm.820150212.
[18] M. Bacanli, S.A. Dilsiz, N. Başaran, et al., Effects of phytochemicals against diabetes, Adv. Food Nutr. Res. 89 (2019) 209–238, https://doi.org/10.1016/bs.afnr.2019.02.006.
[19] M. Kong, K. Xie, M. Lv, et al., Anti-inflammatory phytochemicals for the treatment of diabetes and its complications: lessons learned and future promise, Biomed. Pharmacother. 133 (2021), https://doi.org/10.1016/j.biopha.2020.110975, 110975.
[20] S. Sadrefozalayi, F. Farokhi, Effect of the aqueous extract of Foeniculum vulgare (fennel) on the kidney in experimental PCOS female rats, Avicenna. J. Phytomed. 4 (2014) 110–117.
[21] A. Drzazga, M. Okulus, M. Rychlicka, et al., Lysophosphatidylcholine containing anisic acid is able to stimulate insulin secretion targeting G protein coupled receptors, Nutrients 12 (2020), 1173, https://doi.org/10.3390/nu12041173.

[22] A.A. Sayed, Ferulsinaic acid modulates SOD, GSH, and antioxidant enzymes in diabetic kidney, Evid. Based. Complement. Alternat. Med. (2012), 580104, https://doi.org/10.1155/2012/580104, 2012.
[23] Y. Kohsaka, K. Nagai, Controls and effects of monomer junctions and sequences in curable and degradable polyarylate containing acrylate moieties, Macromol. Rapid Commun. (2020), e2000570, https://doi.org/10.1002/marc.202000570.
[24] J.Z. Wu, Y. Yang, S. Li, et al., Glucose-sensitive nanoparticles based on poly(3-acrylamidophenylboronic acid-block-N-Vinylcaprolactam) for insulin delivery, Int. J. Nanomed. 14 (2019) 8059–8072, https://doi.org/10.2147/IJN.S220936.
[25] J. Li, L. Yang, X. Fan, et al., Multi-responsive behaviors of copolymers bearing N-isopropylacrylamide with or without phenylboronic acid in aqueous solution, Polymers 10 (2018), 293, https://doi.org/10.3390/polym10030293.
[26] X. Si, W. Song, S. Yang, et al., Glucose and pH dual-responsive nanogels for efficient protein delivery, Macromol. Biosci. 19 (2019), e1900148, https://doi.org/10.1002/mabi.201900148.
[27] Q. Guo, Z. Wu, X. Zhang, et al., Phenylboronate-diol crosslinked glycopolymeric nanocarriers for insulin delivery at physiological pH, Soft Matter 10 (2014) 911–920, https://doi.org/10.1039/c3sm52485j.
[28] C. Zheng, Q. Guo, Z. Wu, et al., Amphiphilic glycopolymer nanoparticles as vehicles for nasal delivery of peptides and proteins, Eur. J. Pharmaceut. Sci. 49 (2013) 474–482, https://doi.org/10.1016/j.ejps.2013.04.027.
[29] L. Luo, Preparation and *in Vitro* Release of Insulin-Loaded Chitosan-Phenylboronic Acid Graft [D], 2018. Jinan. University.
[30] G. Cui, K. Zhao, K. You, et al., Synthesis and characterization of phenylboronic acid-containing polymer for glucose-triggered drug delivery, Sci. Technol. Adv. Mater. 21 (2019) 1–10, https://doi.org/10.1080/14686996.2019.1700394.
[31] J. Li, L. Yang, X. Fan, et al., Multi-responsive behaviors of copolymers bearing N-isopropylacrylamide with or without phenylboronic acid in aqueous solution, Polymers 10 (2018), 293, https://doi.org/10.3390/polym10030293.
[32] Q. Wang, M. Fu, Y. Guan, et al., Mechanistic insights into the novel glucose-sensitive behavior of P (NIPAM-co-2-AAPBA), Sci. China Chem. 63 (2020) 377–385, https://doi.org/10.1007/s11426-019-9680-6.
[33] F. Xu, G. Liu, Q. Zhang, et al., A comparative study on two phenylboronic acid based glucose-sensitive hydrogels, Front. Biosci. 2 (2010) 657–667, https://doi.org/10.2741/e121.
[34] F. Fonseca-Wollheim, The influence of pH and various anions on the distribution of NH4+ in human blood, Eur. J. Clin. Chem. Clin. Biochem. 33 (1995) 289–294, https://doi.org/10.1515/cclm.1995.33.5.289. PMID: 7578608.
[35] A. Matsumoto, S. Ikeda, A. Harada, et al., Glucose-responsive polymerbearing a novel phenylborate derivative as a glucose-sensing moiety operating at physiological pH conditions, Biomacromolecules 4 (2003) 1410–1416, https://doi.org/10.1021/bm0345413.
[36] X. Lu, Y. Li, W. Feng, et al., Self-healing hydroxypropyl guar gum/poly (acrylamide-co-3-acrylamidophenyl boronic acid) composite hydrogels with yield phenomenon based on dynamic PBA ester bonds and H-bond, Colloids Surf., A 561 (2019) 325–331, https://doi.org/10.1016/j.colsurfa.2018.10.071.
[37] Q. Wang, H. Wang, Q. Chen, et al., Glucose-Triggered Micellization of Poly (ethylene glycol)-b-poly (N-isopropylacrylamide-co-2-(acrylamido) phenylboronic acid) Block Copolymer, ACS Appl. Polym. Mater. 2 (2020) 3966–3976, https://doi.org/10.1021/acsapm.0c00635.
[38] M. Morey, A. Srivastava, A. Pandit, Glucose-responsive gene delivery at physiological pH through tertiary-amine stabilized boronate-PVA particles synthesized by one-pot reaction, Pharmaceutics 13 (2021) 62, https://doi.org/10.3390/pharmaceutics13010062.
[39] Y. Xue, W. Shi, B. Zhu, et al., Polyethyleneimine-grafted boronate affinity materials for selective enrichment of cis-diol-containing compounds, Talanta 140 (2015) 1–9, https://doi.org/10.1016/j.talanta.2015.03.008.
[40] X. Xu, H. Shang, T. Zhang, et al., A stimuli-responsive insulin delivery system base on reversible phenylboronate modified cyclodextrin with glucose triggered host-guest interaction, Int. J. Pharm. 548 (2018) 649–658, https://doi.org/10.1016/j.ijpharm.2018.07.020.
[41] R. Klopfleisch, F. Jung, The pathology of the foreign body reaction against biomaterials, J. Biomed. Mater. Res. A. 105 (2017) 927–940, https://doi.org/10.1002/jbm.a.35958.
[42] X. Zhang, S. Lü, C. Gao, et al., Highly stable and degradable multifunctional microgel for self-regulated insulin delivery under physiological conditions, Nanoscale 5 (2018) 6498–6506, https://doi.org/10.1039/c3nr00835e.
[43] H. Guo, H. Li, J. Gao, et al., Phenylboronic acid-based amphiphilic glycopolymeric nanocarriers for *in vivo* insulin delivery, Polym. Chem-UK 7 (2016) 3189–3199, https://doi.org/10.1039/C6PY00131A.
[44] T. Elshaarani, H. Yu, L. Wang, et al., Chitosan reinforced hydrogels with swelling-shrinking behaviors in response to glucose concentration, Int. J. Biol. Macromol. 161 (2020) 109–121, https://doi.org/10.1016/j.ijbiomac.2020.06.012.
[45] L. Zhao, C. Xiao, J. Ding, et al., Competitive binding-accelerated insulin release from a polypeptide nanogel for potential therapy of diabetes, Polym. Chem-UK 6 (2015) 3807–3815, https://doi.org/10.1039/C5PY00207A.
[46] L. Zhao, C. Xiao, L. Wang, et al., Glucose-sensitive polymer nanoparticles for self-regulated drug delivery, Chem, Commun. Now. 52 (2016) 7633–7652, https://doi.org/10.1039/c6cc02202b.
[47] T. Elshaarani, H. Yu, L. Wang, et al., Chitosan reinforced hydrogels with swelling-shrinking behaviors in response to glucose concentration, Int. J. Biol. Macromol. 161 (2020), https://doi.org/10.1016/j.ijbiomac.2020.06.012 https://doi.org/10.109-121.
[48] H.W. Rodbard, D. Rodbard, Biosynthetic human insulin and insulin analogs, Am. J. Therapeut. 27 (2020) e42–e51, https://doi.org/10.1097/MJT.0000000000001089.
[49] M. Czarnecka, M. Świtalska, J. Wietrzyk, et al., Synthesis, characterization, and *in vitro* cancer cell growth inhibition evaluation of novel phosphatidylcholines with anisic and veratric acids, Molecules 23 (2018), 2022, https://doi.org/10.3390/molecules23082022.
[50] Y. Zhang, J. Yang, J. Zhang, et al., A bio-inspired injectable hydrogel as a cell platform for real-time glycaemic regulation, J. Mater. Chem. B. 8 (2020) 4627–4641, https://doi.org/10.1039/d0tb00561d.
[51] M. Caprnda, D. Mesarosova, P.F. Ortega, et al., Glycemic variability and vascular complications in patients with type 2 diabetes mellitus, Folia Med. (Plovdiv) 59 (2017) 270–278, https://doi.org/10.1515/folmed-2017-0048.
[52] K. Furuichi, M. Shimizu, A. Hara, et al., Diabetic nephropathy: a comparison of the clinical and pathological features between the CKD risk classification and the classification of diabetic nephropathy 2014 in Japan, Intern. Med. 57 (2018) 3345–3350, https://doi.org/10.2169/internalmedicine.1132-18.
[53] L. Kishore, N. Kaur, R. Singh, Distinct biomarkers for early diagnosis of diabetic nephropathy, Curr. Diabetes Rev. 13 (2017) 598–605, https://doi.org/10.2174/1573399812666161207123007.
[54] E.A. Christofides, N. Desai, Optimal early diagnosis and monitoring of diabetic kidney disease in type 2 diabetes mellitus: addressing the barriers to albuminuria testing, J. Prim. Care. Commun. Health. 12 (2021), 215, https://doi.org/10.1177/21501327211003683.
[55] J.C. Jha, C. Banal, B.S. Chow, et al., Diabetes and kidney disease: role of oxidative stress, Antioxidants Redox Signal. 25 (2016) 657–684, https://doi.org/10.1089/ars.2016.6664.
[56] S.K. Sinha, S.B. Nicholas, J.H. Sung, et al., Hs-CRP is associated with incident diabetic nephropathy: findings from the jackson heart study, Diabetes Care 42 (2019) 2083–2089, https://doi.org/10.2337/dc18-2563.
[57] S. Karadag, E. Sakci, S. Uzun, et al., The correlation of inflammatory markers and plasma vaspin levels in patients with diabetic nephropathy, Ren. Fail. 38 (2016) 1044–1049, https://doi.org/10.1080/0886022X.2016.1183444.
[58] H. Yang, T. Xie, D. Li, et al., Tim-3 aggravates podocyte injury in diabetic nephropathy by promoting macrophage activation via the NF-κB/TNF-α pathway, Mol. Metabol. 23 (2019) 24–36, https://doi.org/10.1016/j.molmet.2019.02.007.